

Dislocation mechanism of $Ni_{47}Co_{53}$ alloy during rapid solidification

Yun-Chun Liu(刘云春), Yong-Chao Liang(梁永超), Qian Chen(陈茜), Li Zhang(张利), Jia-Jun Ma(马家君), Bei Wang(王蓓), Ting-Hong Gao(高廷红), and Quan Xie(谢泉)

Citation: Chin. Phys. B, 2023, 32 (**6**): 066104. DOI: 10.1088/1674-1056/aca7ea
Journal homepage: http://cpb.iphy.ac.cn; http://iopscience.iop.org/cpb

What follows is a list of articles you may be interested in

Atomic simulations of primary irradiation damage in U-Mo-Xe system

Wen-Hong Ouyang(欧阳文泓), Jian-Bo Liu(刘剑波), Wen-Sheng Lai(赖文生),Jia-Hao Li(李家好), and Bai-Xin Liu(柳百新)

Chin. Phys. B, 2023, 32 (**3**): 036101. DOI: 10.1088/1674-1056/ac9366

Structural evolution and molecular dissociation of H_2S under high pressures

Wen-Ji Shen(沈文吉), Tian-Xiao Liang(梁天笑), Zhao Liu(刘召), Xin Wang(王鑫), De-Fang Duan(段德芳), Hong-Yu Yu(于洪雨), and Tian Cui(崔田)

Chin. Phys. B, 2022, 31 (**7**): 076102. DOI: 10.1088/1674-1056/ac5980

Evolution of defects and deformation mechanisms in different tensile directions of solidified lamellar Ti-Al alloy

Yutao Liu(刘玉涛), Tinghong Gao(高廷红), Yue Gao(高越), Lianxin Li(李连欣), Min Tan(谭敏), Quan Xie(谢泉), Qian Chen(陈茜), Zean Tian(田泽安), Yongchao Liang(梁永超), and Bei Wang(王蓓)

Chin. Phys. B, 2022, 31 (**4**): 046105. DOI: 10.1088/1674-1056/ac1f0b

First-principles study of two new boron nitride structures: C12-BN and O16-BN

Hao Wang(王皓), Yaru Yin(殷亚茹), Xiong Yang(杨雄), Yanrui Guo(郭艳蕊), Ying Zhang(张颖), Huiyu Yan(严慧羽), Ying Wang(王莹), and Ping Huai(怀平)

Chin. Phys. B, 2022, 31 (**2**): 026102. DOI: 10.1088/1674-1056/ac0a69

Polymorph selection of magnesium under different pressures: A simulation study

Wei Liu(刘维), Boqiang Wu(吴博强), Ze'an Tian(田泽安), Yunfei Mo(莫云飞), Tingfei Xi(奚廷斐), Zhiyi Wan(万子义), Rangsu Liu(刘让苏), and Hairong Liu(刘海蓉)

Chin. Phys. B, 2022, 31 (**1**): 016103. DOI: 10.1088/1674-1056/ac2e5e

---

Dislocation mechanism of $Ni_{47}Co_{53}$ alloy during rapid solidification

Yun-Chun Liu(刘云春), Yong-Chao Liang(梁永超)†, Qian Chen(陈茜), Li Zhang(张利), Jia-Jun Ma(马家君), Bei Wang(王蓓), Ting-Hong Gao(高廷红), and Quan Xie(谢泉)

Institute of Advanced Optoelectronic Materials and Technology, School of Big Data and Information Engineering, Guizhou University, Guiyang 550025, *China*

(Received 16 September 2022; revised manuscript received 8 November 2022; accepted manuscript online 2 December 2022)

Dislocations and other atomic-level defects play a crucial role in determining the macroscopic properties of crystalline materials, but it is extremely difficult to observe the evolution of dislocations due to the limitations of the most advanced experimental techniques. Therefore, in this work, the rapid solidification processes of $Ni_{47}Co_{53}$ alloy at five cooling rates are studied by molecular dynamics simulation, and the evolutions of their microstructures and dislocations are investigated as well. The results show that face-centered cubic (FCC) structures are formed at the low cooling rate, and the crystalline and amorphous mixture appear at the critical cooling rate, and the amorphous are generated at the high cooling rate. The crystallization temperature and crystallinity decrease with cooling rate increasing. Dislocations are few at the cooling rates of 1×10^{11} K/s, 5×10^{12} K/s, and 1×10^{13} K/s, and they are most abundant at the cooling rates of 5×10^{11} K/s and 1×10^{12} K/s, in which their dislocation line lengths are both almost identical. There appear a large number of dislocation reactions at both cooling rates, in which the interconversion between perfect and partial dislocations is primary. The dislocation reactions are more intense at the cooling rate of 5×10^{11} K/s, and the slip of some dislocations leads to the interconversion between FCC structure and hexagonal close packed (HCP) structure, which causes the twin boundaries (TBs) to disappear. The FCC and HCP are in the same atomic layer, and dislocations are formed at the junction due to the existence of TBs at the cooling rate of 1×10^{12} K/s. The present research is important in understanding the dislocation mechanism and its influence on crystal structure at atomic scales.

Keywords: molecular dynamics simulation, rapid solidification, crystal structure, dislocation interaction

PACS: 61.72.Lk, 87.10.Tf, 81.30.Fb, 91.60.Ed **DOI:** 10.1088/1674-1056/aca7ea

1. Introduction

Ni–Co alloys are an important engineering material, which are commonly used for functional and decorative coatings in connectors, turbines, microelectronics, and medical devices due to their superior hardness, wear resistance, magnetic properties, and corrosion resistance.[1–3] However, processing parameters such as Co salt density and current density in the plating solution have important effects on the morphology and abrasion properties of Ni–Co coatings.[4] In fact, the yield and tensile strength can be increased by increasing Co content, but the fracture resistance and ductility will be reduced,[5] thereby limiting its practical application. It was found that the activity of crystal defects can improve the mechanical properties, such as point defects, line defects, and surface defects.[6] As line defects in the crystal structure, dislocations are the carriers of plastic deformation in metallic materials, so the generation and evolution of dislocations and the interaction between dislocations can affect the mechanical properties.[7–9] Therefore, the investigation of dislocations can optimize the properties of materials on an atomic scale.

Dislocation theories play a key role in studying plastic deformation and strength of materials, which have attracted the attention of many researchers. Lu *et al.*[10] found that $1/6\langle112\rangle$ (Shockley) partial dislocations are dissociated by perfect dislocations on twin boundaries, and these partial dislocations can slide on the twin boundaries and lead to plastic deformation, thereby increasing ductility. Laplanche *et al.*[11] and Miao *et al.*[12] studied the deformation behavior of CrCoNi alloy, where the planar slip of dislocations and the dissociation of $1/2\langle110\rangle$ (perfect) dislocations on the $\{111\}$ plane into $1/6\langle112\rangle$ (Shockley) partial dislocations affect the deformation behavior in the early stages. In Zhang *et al.*'s study,[13] the substrate stacking faults started from the lattice mismatch region and evolved into B-type face-centered cubic (FCC) sheets at the relaxed P-type HCP/FCC (where HCP stands for hexagonal close packed) interface, and then the mismatch region provided a source of nucleation for perfect dislocations. The interactions between dislocations also play a vital role in functional materials such as shape memory alloys (SMAs), dictating the rate of slip emission from disconnected on twin boundaries, which ultimately manifest in the damping and fatigue response of SMAs.[14]

Dislocations are also essential for crystal growth, and the formation of dislocations during crystal growth has been studied by numerous researchers. Zhou *et al.*[15] investigated the directional growth of Si, and they found that there are no dislocations formed as growing along the [100] and [110] directions, while multiple dislocations are formed as growing along the [112] direction, which are identified as a partial dislocation located on the $\{111\}$ plane. Ryningen *et al.*[16] found

†Corresponding author. E-mail: 20113248@qq.com

© 2023 Chinese Physical Society and IOP Publishing Ltd

that dislocation clusters can be formed during the growth of polysilicon, and the number of dislocations in the dislocation clusters increases with the growth of polysilicon. The interactions of He with dissociated screw dislocations in fcc Ni were investigated by Xu *et al.*,[17] and they found that interstitial He atoms at tetrahedral sites in the perfect fcc lattice and atoms occupying one plane above or below one of the two Shockley partial cores exhibit the strongest binding energy. Recently, the first principles method has been used to study the strengthening effect of alloying elements Re, Ta, and W in the γ/γ' interface [110] (001) dislocation core.[18] By analyzing the substitution formation energy and alloy-element migration energy, it was found that the stability of [110] (001) dislocation core is enhanced by adding Ta, W, and Re. Rapid solidification was widely used as an important material preparation method to enhance their properties.[19–21] However, it is greatly difficult to reveal the dislocation mechanism experimentally during rapid solidification, which limits the study of dislocations on an atomic scale. Therefore, in this study, the dislocations and their reaction mechanism of Ni–Co alloy are investigated during rapid solidification by molecular dynamics (MD) method, which is important in further understanding the microstructure and its evolution.

2. Simulation conditions and methods

In this study, MD simulations of the rapid solidification process of $Ni_{47}Co_{53}$ alloy[22] at five cooling rates were performed by using a large-scale atomic/molecular parallel simulator (LAMMPS).[23] The embedded-atom method (EAM) established by Pun *et al.*[24] was used to describe the interactions among atoms. In the EAM, the total energy E_i of an atom i is represented by

$$E_i = F_\alpha \sum_{j\neq i} \rho_\beta(r_{ij}) + \frac{1}{2}\sum_{j\neq i} \phi_{\alpha\beta}(r_{ij}), \tag{1}$$

where α and β are the element types of the center atom i and the neighboring atom j, F_α is the embedding function of α, ρ_β is the charge density function of β, r_{ij} is the distance between atoms i and j, $\phi_{\alpha\beta}$ is the pair potential function between α and β.

The lattice parameters and formation energy fitted with the EAM are listed in Table 1, and compared with the first principle data, the results are generally consistent. References [24,26,27] provided the specific construction method of EAM, and the EAM has been verified to be suitable for Ni–Co system and it can effectively simulate the dislocation behaviors.[28,29]

Table 1. Lattice constants and formation energy values of imaginary phases of Co–Ni system obtained from the present EAM potential in comparison with first-principles data.[25] In the table, the numbers marked by an asterisk are used in the potential fit, and remaining numbers are predictions of the potential. The formation energy is in units of eV/atom.

Phase	Structure	Lattice parameter (a,c) (Å)		Formation energy	
		Ab initio	EAM	*Ab initio*	EAM
CoNi	B1	5.042 67	4.913 11	0.755 80*	0.646 24
	B2	2.791 75	2.922 41	0.138 60*	0.152 09
	B_h[a]	2.475 14, 4.032 98	2.439 83, 4.3795	−0.01530*	−0.04390
	L1	3.568 91, 3.461 30	3.690 74, 3.587 06	−0.01160*	−0.00962
$CoNi_3$	$L1_2$	3.497 65	3.609 25	0.002 90*	0.004 11
Co_3Ni	$L1_2$	3.496 99*	3.621 63	−0.01780*	−0.01213

[a]WC prototype.

The 10^4 atoms (4700 Ni atoms and 5300 Co atoms) were randomly placed in a cubic box with periodic boundaries in three directions. The simulation process was performed under NPT synthesis in time steps of 1 fs. The starting temperature was set to 1800 K (the alloy melting point is about 1200 K to 1375 K[30]), and the isothermal relaxation of 1 ns at this temperature took place to ensure that the system is in a full equilibrium state. Subsequently, the system was solidified to a specified temperature of 300 K at five different cooling rates (1×10^{11} K/s, 5×10^{11} K/s, 1×10^{12} K/s, 5×10^{12} K/s, and 1×10^{13} K/s), and finally five models were obtained. During the simulation, the Nose–Hoover thermostat method[31,32] was used to control the temperature and the Parrinello–Rahman algorithm[33] to control the pressure (0 GPa). And thermodynamic information such as coordinate, velocity, and energy of the atoms are recorded every 1 K for subsequent microstructure analysis.

The simulation results were analyzed and visualized by the open visualization tool (OVITO),[34] where the evolution of microstructure and the combination and dissociation of dislocations were identified by the common neighbor analysis (CNA)[35] and the dislocation extraction algorithm (DXA).[36]

3. Results and discussion

3.1. Average potential energy

The energy–temperature (E–T) curve can intuitively describe the basic characteristics during rapid solidification. In general, the potential energy decreases linearly as the temperature decreases, with a sudden drop at a certain temperature,

i.e., a phase transition, and the discontinuous change in potential energy often occurs during liquid–solid transition.[37] Figure 1 shows the E–T curves of $Ni_{47}Co_{53}$ alloy at five cooling rates during rapid solidification. For the cooling rates of 1×10^{11} K/s, 5×10^{11} K/s, and 1×10^{12} K/s, the E–T curves exhibit obvious inflection points with temperature decreasing, indicating that crystallization transition occurs at these cooling rates. The temperatures corresponding to these inflection points are values of the crystallization transition temperature T_c of the systems, which are $T_{c1} = 1504$ K, $T_{c2} = 1440$ K, $T_{c3} = 1300$ K, respectively. For the cooling rates of 5×10^{12} K/s and 1×10^{13} K/s, there are no significant abrupt changes in the E–T curves, and their slopes change at $T = 1140$ K and $T = 910$ K, respectively, suggesting that there are no obvious crystallization transitions in these two systems.

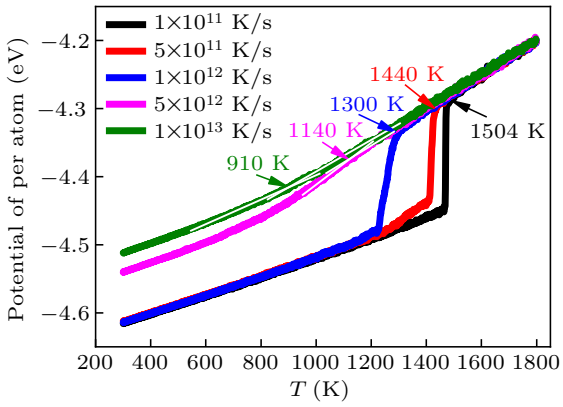


Fig. 1. Curves of average potential energy *versus* temperature at five cooling rates.

3.2. The $g(r)$ function

The $g(r)$ function is the Fourier transform of structure factor $S(q)$ obtained from systematic x-ray diffraction,[38] which represents the probability of finding an adjacent atom at a distance r from the central atom. It is commonly used as a statistical analysis to describe the order of the microstructure. For an ideal crystal structure, the curve behaves as a pulse, but owing to the thermal motion of the atoms, the curve is usually a spike with a certain width.[39]

The $g(r)$ curves at five cooling rates are displayed in Fig. 2. The initial structures of five systems after isothermal relaxation are consistent with each other, when the temperature drops to 300 K, the $g(r)$ curves show sharp peaks at the cooling rates of 1×10^{11} K/s, 5×10^{11} K/s, and 1×10^{12} K/s, which is significant feature of the crystal structure, indicating that these systems form crystal structures. For the cooling rate 5×10^{12} K/s, the height of the peak is quite small and there exists short-range orderliness, which is an intermediate state between crystalline and amorphous, and the cooling rate is defined as the critical cooling rate (CCR).[21,40] At the fastest cooling rate of 1×10^{13} K/s, the second peak of the $g(r)$ curve splits into two sub-peaks, which is typical feature of the spatial distribution in the amorphous system, implying that the system forms amorphous structure.

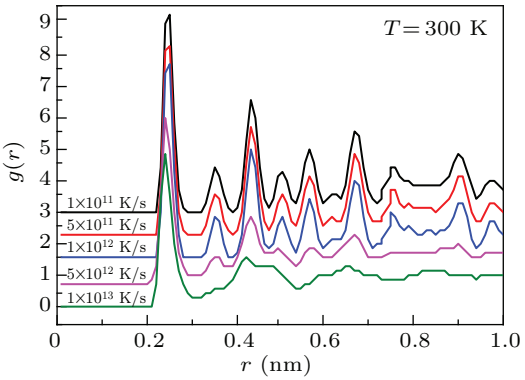


Fig. 2. Curves of $g(r)$ *versus* r of the system at five cooling rates.

3.3. Cluster analysis

In order to investigate the microstructure of $Ni_{47}Co_{53}$ alloy during rapid solidification, the variation of clusters with temperature are shown in Fig. 3. For convenience, the clusters except FCC, HCP and BCC are called the other. Since the number of BCC is extremely small at five cooling rates, the analysis focuses on the variation of FCC and HCP.

As illustrated in Fig. 3(a), the other decreases rapidly at T_{c1}, and the FCC increases immediately at the cooling rate of 1×10^{11} K/s. The FCC accounts for 96.71% at $T = 300$ K, indicating that a near-perfect FCC crystal structure is formed. It is noteworthy that the amount of HCP also starts to increase at T_{c1}, reaching 3.57% at $T = 1488$ K, and then decreases rapidly to 0.1% at $T = 1485$ K. This is because HCP is sub-stable and it is easy to transform into FCC under thermal stress. Eventually HCP reaches 0.8% and forms a stacking fault (SF). At the cooling rate of 5×10^{11} K/s, the other starts to decrease at T_{c2}, while FCC and HCP also begin to increase. When the temperature decreases to 1413 K, HCP increases to 8.02%, and at this moment multiple HCP twin boundaries (TBs) are formed, which is demonstrated in Fig. 3(b). HCP decreases to 1.59% at $T = 1250$ K, and FCC increases to 78.3% and then it keeps increasing at a flat rate. Eventually, FCC reaches 93.01%, while the HCP number decreases to 0.7%, and the TBs disappear, forming a relatively perfect FCC crystal.

At the cooling rate of 1×10^{12} K/s, the other decreases sharply at T_{c3}, while FCC increases to 65.8% and HCP reaches 9.19% when the temperature drops to 1225 K. Unlike the previous cooling rates, HCP does not increase and then decrease, but slowly increases to a certain value and then stays stable. Finally, HCP reaches 10.5% at $T = 300$ K, which exists in FCC crystal in the form of TBs as shown in Fig. 3(c). For the cooling rate of 5×10^{12} K/s, FCC and HCP slowly increase at $T = 1140$ K as shown in Fig. 3(d), and they eventually increase to 26.68% and 7.36%, respectively. As the critical cooling rate, it is in a state where the crystalline and amorphous

coexist. As is well known, amorphous structures, also known as metallic glasses (MGs), are frozen liquids with amorphous atoms by bypassing crystallization during solidification.[41] Only when the cooling rate is fast enough to avoid crystallizing, that is, the cooling rate is faster than the CCR, can MGs be formed. As shown in Fig. 3(e), MGs are formed because the cooling rate is higher than the CCR and the atoms cannot rearrange in time to form a crystal structure.

Figure 3(f) shows the curve of degree of crystallinity *versus* cooling rate at five cooling rates, where the crystallinity is defined as the sum of crystallinities of FCC, HCP, and BCC. Although the crystallinity gradually decreases as the cooling rate increases in general, the crystallinity at the cooling rate of 1×10^{12} K/s is slightly higher than that at the cooling rate of 5×10^{11} K/s. This is because two systems are not fully crystallized, the other accounts for 6.2% at the cooling rate of 5×10^{11} s and 5.5% at the cooling rate of 1×10^{12} K/s. These regions where the other atoms aggregates are unstable and have higher energy, resulting in a lower crystallinity at the cooling rate of 5×10^{11} K/s. In short, the systems of lower cooling rates are more likely to form perfect crystalline structures, and the systems of higher cooling rates prefer to form amorphous structures.

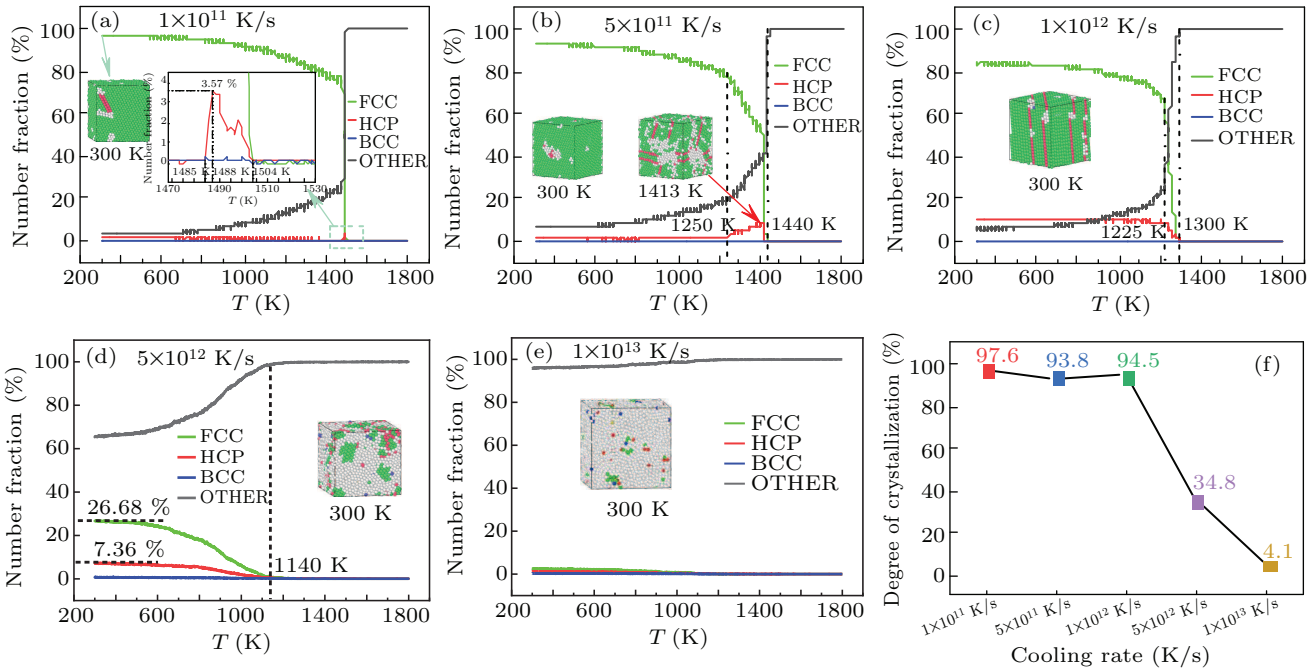


Fig. 3. Variations of clusters in the systems for five cooling rates: (a) 1×10^{11} K/s, (b) 5×10^{11} K/s, (c) 1×10^{12} K/s, (d) 5×10^{12} K/s, (e) 1×10^{13} K/s; (f) crystallinity for five cooling rates, with colors in the visualization diagram representing FCC (green), HCP (red), BCC (blue), and the other (gray).

3.4. Dislocation analysis

During crystallization, the crystals are subjected to impurities, temperature changes or vibration stress, or mechanical stress such as hitting, cutting, grinding, which deforms the internal arrangement and causes the atomic rows to slip away from each other. It no longer conforms with the orderly arrangement for ideal crystal, resulting in a one-dimensional defect called dislocation.[42] According to classical nucleation theory (CNT),[43,44] a crystalline cluster of any size is considered as a macroscopic object, and once the nuclei reaches a critical size, it continues to grow until all the liquid solidifies or it encounters another growing crystal. Rapid solidification is a homogeneous nucleation process, in which there will be different sizes of nuclei, but only one of which is stable, the others are metastable. Dislocations can be located in grain boundaries and steadily growing into nuclei. The generation of dislocations is closely related to the rapid solidification process.[45] On the one hand, the fast quenching of the melts increases the significant concentration of vacancies, and a large number of vacancies become the origin of dislocations. On the other hand, the thermal stress and phase transition stress inside the alloy not only induce the dislocations to form, but also cause the dislocations to move and proliferate, which results in the gather and collapse of vacancies.

3.4.1. Dislocation length

The total length of dislocation lines at five cooling rates are calculated by the dislocation extraction algorithm (DXA), and the results are shown in Fig. 4. It is evident that the temperature at which dislocations appear first decrease as the cooling rate increases, and finally the total lengths of the dislocation lines fluctuate around a certain value. At the cooling rate of 1×10^{11} K/s, dislocations appear at 1503 K, indicating that the system starts to crystallize. In the crystallization process, the total dislocation length fluctuates greatly and finally stays at about 100 Å. The two systems show dislocations first at

1430 K and 1290 K at the cooling rates of 5×10^{11} K/s and 1×10^{12} K/s, respectively. The fluctuations of the two dislocation curves are extremely strong in the crystallization interval, which means that the microstructure evolution is very intense at this time. In addition, the fluctuation range at 5×10^{11} K/s is wider than that at 1×10^{12} K/s, which means that the variation at 5×10^{11} K/s is more complex and lasts longer. Interestingly, the two dislocation curves are stable at around 325 Å finally. For the cooling rates of 5×10^{12} K/s and 1×10^{13} K/s, they first to show dislocations at 1135 K and 990 K, respectively. At the cooling rate of 5×10^{12} K/s, the dislocation length fluctuates around 50 Å. Dislocation length is a minimum value and almost close to 0 at the cooling rate of 1×10^{13} K/s. The reason for this is that the MGs have few crystals and their dislocation lines are short.

From the above, it is clear that the cooling rate has an important influence on the dislocation arrangement.[46] Both high cooling system and low cooling system have few dislocations, and the intermediate cooling system has the most dislocations. This is due to the fact that the more perfect crystal structures are formed at the lower cooling rate, and the amorphous structures are formed at the higher cooling rate, both of which are hard to generate dislocations. However, the imperfect crystalline structure and polycrystalline structure are formed at the intermediate cooling rate, which have more dislocations.

Figure 5 shows the dislocation distributions for the five systems at $T = 300$ K. The dislocations are fewer and mainly concentrated in two sites containing $1/6\langle112\rangle$ (Shockley), $1/6\langle110\rangle$ (stair-rod), and $1/3\langle111\rangle$ (Frank) at the cooling rate of 1×10^{11} K/s. The dislocations are intertwined and spiral at the cooling rate of 5×10^{11} K/s, and the dislocation types are mainly $1/6\langle112\rangle$ (Shockley) and $1/2\langle110\rangle$ (perfect), and there are a large number of dislocation loops (DLs).[47] At the cooling rate of 1×10^{12} K/s, the dislocations are mainly distributed around the TBs, which show long stripes, with $1/6\langle112\rangle$ (Shockley) dominating. At the cooling rates of 5×10^{12} K/s and 1×10^{13} K/s, the dislocation lines are short and small, scattered and limited.

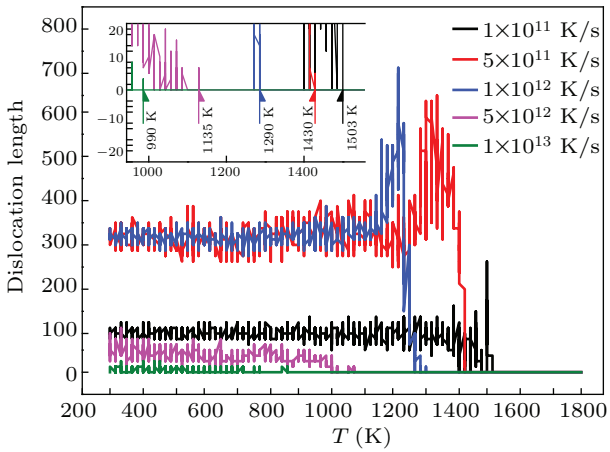


Fig. 4. Variations of total length of dislocation with temperature at five cooling rates.

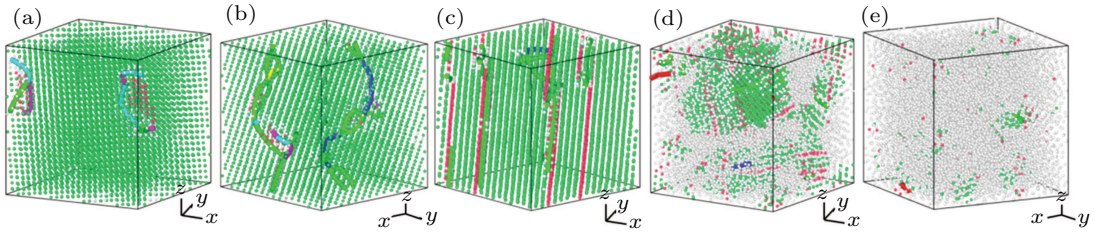


Fig. 5. Dislocation distributions at 300 K for five cooling rates: (a) 1×10^{11} K/s, (b) 5×10^{11} K/s, (c) 1×10^{12} K/s, (d) 5×10^{12} K/s, (e) 1×10^{13} K/s, with cluster colors representing FCC (green), HCP (red), other (grey), and with dislocation colors denoting $1/6\langle112\rangle$ (Shockley, green), $1/2\langle110\rangle$ (perfect blue), $1/3\langle111\rangle$ (Frank cyan), fuchsia $1/6\langle110\rangle$ (Stair-rod, fuchsia), $(1/3\langle001\rangle$ (Hirth, yellow), other (red).

In summary, the dislocation lengths at the cooling rates of 5×10^{11} K/s and 1×10^{12} K/s are almost the same. The system at the cooling rate of 5×10^{11} K/s has a lower crystallinity, resulting in more unstable high-energy regions, where a number of dislocations are formed. And the system at the cooling rate of 1×10^{12} K/s has also a high dislocation density due to polycrystal containing dislocation for itself. To further investigate the dislocation changes within these two systems, their dislocation evolution and interaction are discussed below.

3.4.2. Dislocation evolution

Figures 6(a) and 6(b) demonstrate the evolution of the dislocations at some specific temperatures during rapid solidification at the cooling rates of 5×10^{11} K/s and 1×10^{12} K/s, respectively. It is observed that six different types of dislocations exist in the two systems during solidification, where the $1/6\langle112\rangle$ (Shockley) partial dislocation occupies a significant proportion. As Shockley dislocations are slip dislocations, the slip surface in FCC is the $\{111\}$ close-packed plane, where the slip of a perfect dislocation requires higher energy and leads to greater lattice distortion than the combined slip of two partial dislocations. Therefore, partial dislocations are prone to arise in FCC.[48] At the early stage of crystallization, the dislocations are small and fragmented due to the low crystal content, and $1/6\langle112\rangle$ (Shockley) is the main dislocation. As the solidification process proceeds, the degree of crystallization deepens, and the newly generated dislocations become entangled with the original dislocations increasing. The dislocation lines start to become more and longer and intertwine to form

many dislocation junctions and DLs. A variety of dislocations such as $1/2\langle 110\rangle$ (perfect), $1/6\langle 110\rangle$ (stair-rod) and the other appears. Dislocations are basically stable and will no longer have any dramatic changes finally.

The lengths of all types of dislocations within the two systems are counted by DXA. As shown in Fig. 7, the most of dislocations are $1/6\langle 112\rangle$ (Shockley) partial dislocation in both systems. The dislocation variation is more drastic at the cooling rate of 5×10^{11} K/s, and the floating is more obvious, containing a certain amount of $1/2\langle 110\rangle$ (perfect) (about 40 Å) and $1/6\langle 110\rangle$ (stair-rod) (about 25 Å). And the floating is relatively steady at the cooling rate of 1×10^{12} K/s, while there are some other dislocations in the system, such as $1/18\langle 114\rangle$, $1/18\langle 127\rangle$, and $1/9\langle 122\rangle$. They are TBs generated by stacking fault or the products of the reaction between ordinary dislocations and TBs. In addition to structural changes, the interactions among different types of dislocations are also responsible for the fluctuation.

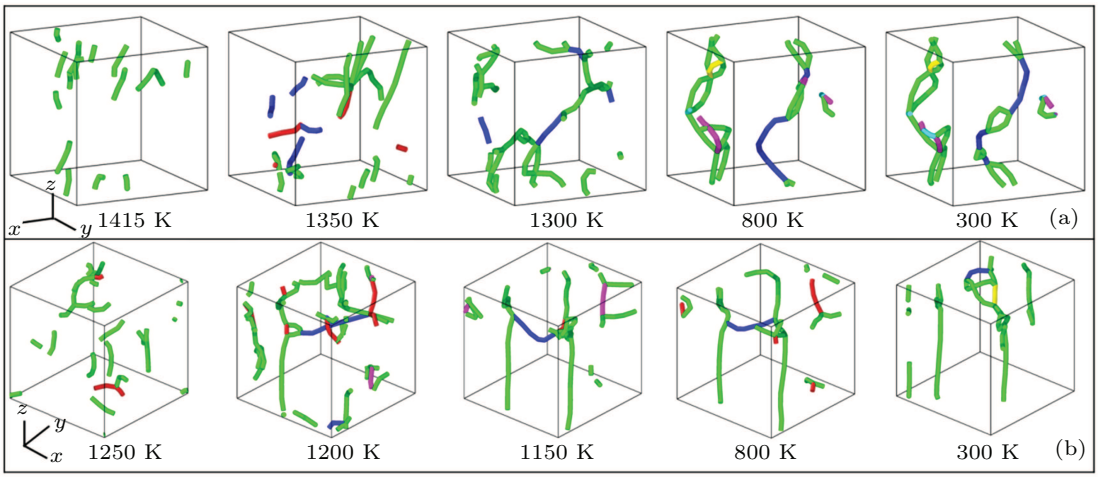


Fig. 6. Evolutions of dislocations during solidification at cooling rate (a) 5×10^{11} K/s and (b) 1×10^{12} K/s, with dislocation colors representing $1/6\langle 112\rangle$ (Shockley, green), $1/2\langle 110\rangle$ (perfect, blue), $1/3\langle 111\rangle$ (Frank, cyan), $1/6\langle 110\rangle$ (Stair-rod, fuchsia), $1/3\langle 001\rangle$ (Hirth, yellow), other (red).

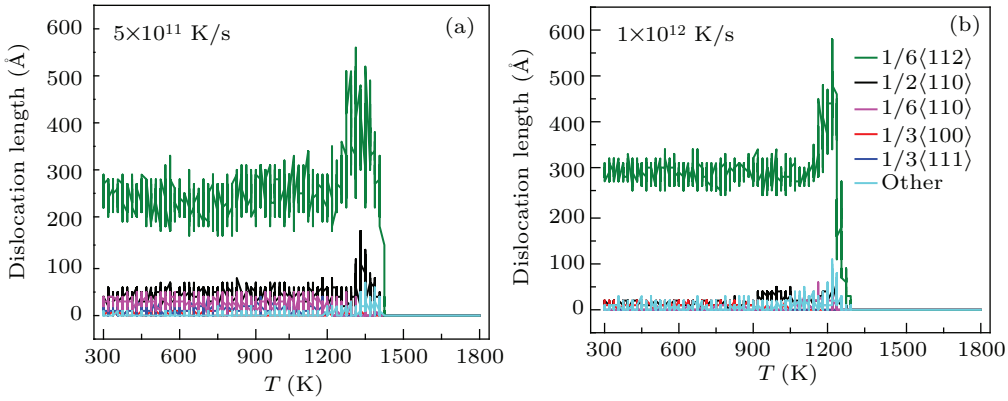


Fig. 7. Plots of dislocation length *versus* temperature of different types of dislocations in systems.

3.4.3. Dislocation interactions

To understand more clearly the interaction between dislocations during rapid solidification, the dislocation distributions at the cooling rates of 5×10^{11} K/s and 1×10^{12} K/s within 914 K–910 K are intercepted as shown in Figs. 8 and 9, respectively. The DXA is used to analyze the combination and dissociation between dislocations. It should be noted that in addition to the Bergers vector conservation condition,[49] all dislocation reactions must satisfy the energy condition[50] as shown below:

$$\sum E_{\text{before}} \geq \sum E_{\text{after}}. \tag{2}$$

In other words, the energy before the reaction will not be less than the energy after the reaction. As can be seen from Fig. 1, the energy of the system continuously decreases, which satisfies the energy condition in the reaction.

In Fig. 8, four different types of dislocations appear in total, and interactions can occur among these dislocations. Two $1/6\langle 112\rangle$ (Shockley) dislocations can react to form a $1/2\langle 110\rangle$ (perfect), and the interaction is reversible. For example, a + b = f follows the equation

$$\frac{1}{6}[121]+\frac{1}{6}[\bar{1}12]=\frac{1}{2}[011], \tag{3}$$

f = k + l follows the equation

$$\frac{1}{2}[011]=\frac{1}{6}[121]+\frac{1}{6}[\bar{1}12], \tag{4}$$

d + e = i follows the equation

$$\frac{1}{6}[112]+\frac{1}{6}[\bar{1}21]=\frac{1}{2}[011], \tag{5}$$

c = g + h follows the equation

$$\frac{1}{2}[0\bar{1}\bar{1}]=\frac{1}{6}[\bar{1}\bar{1}\bar{2}]+\frac{1}{6}[1\bar{2}\bar{1}], \tag{6}$$

j = m + n and o = v + w also follow Eq. (6).

The $1/6\langle 112\rangle$ (Shockley) can react with $1/6\langle 110\rangle$ (stair-rod) to form $1/3\langle 111\rangle$ (Frank). For example,
t = s + r and u = p + q follow the equation

$$\frac{1}{3}[\bar{1}11]=\frac{1}{6}[\bar{1}21]+\frac{1}{6}[\bar{1}01]. \tag{7}$$

Equation (7) is also reversible, for example,

$$\frac{1}{6}[\bar{1}12]+\frac{1}{6}[\bar{1}10]=\frac{1}{3}[\bar{1}11]. \tag{8}$$

Apart from the reaction marked in the figure, there are other dislocation reactions. Two $1/6\langle 112\rangle$ (Shockley) meet and react with each other, a $1/6\langle 110\rangle$ (stair-rod) can be formed, for example,

$$\frac{1}{6}[21\bar{1}]+\frac{1}{6}[\bar{1}\bar{2}1]=\frac{1}{6}[1\bar{1}0]. \tag{9}$$

The $1/2\langle 110\rangle$ (perfect) can be dissociated into a fixed $1/3\langle 111\rangle$ (Frank) and a $1/6\langle 112\rangle$ (Shockley) partial dislocation, for example,

$$\frac{1}{2}[1\bar{1}0]=\frac{1}{3}[1\bar{1}1]+\frac{1}{6}[1\bar{1}\bar{2}]. \tag{10}$$

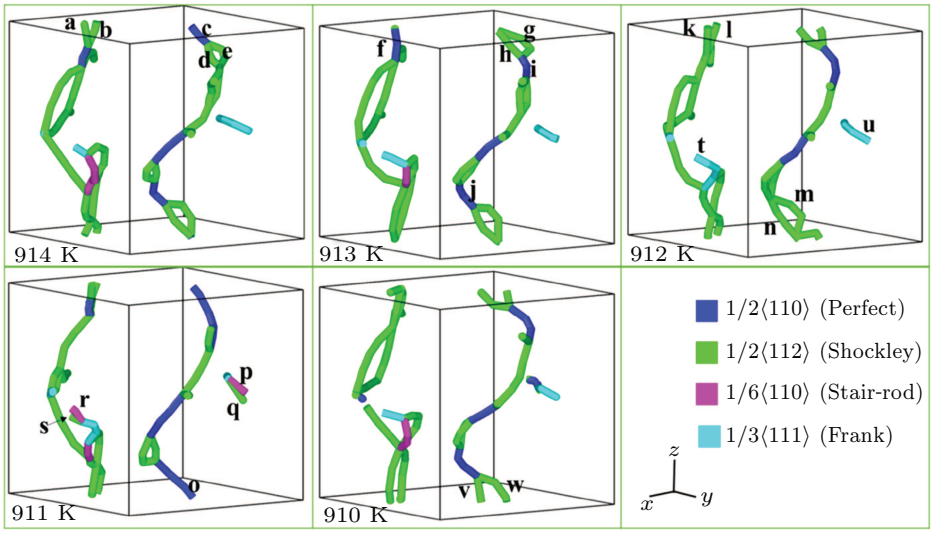


Fig. 8. Dislocation evolutions in a temperature range of 914 K–910 K for the system at cooling rate 5×10^{11} K/s .

In Fig. 9, five different types of dislocations appear, where the other dislocations are a class of dislocations that do not belong to $1/2\langle 110\rangle$ (perfect), nor $1/6\langle 112\rangle$ (Shockley), nor $1/6\langle 110\rangle$ (stair-rod), nor $1/3\langle 100\rangle$ (Hirth), and nor $1/3\langle 111\rangle$ (Frank). The parts of the dislocation lines ① and ② in the same slip plane react with each other, following

$$\frac{1}{6}[1\bar{2}1]+\frac{1}{6}[\bar{1}2\bar{1}]=0. \tag{11}$$

The dislocations vanish because the sum of the Berger vectors is 0. This behavior is called annihilation of dislocations.[51] The unreacted part is the dislocation line ④. The dislocation line ③ is dissociated into dislocation lines ⑤ and ⑥, conforming to the following equation:

$$\frac{1}{6}[112]=\frac{1}{6}[\bar{1}21]+\frac{1}{6}[2\bar{1}1]. \tag{12}$$

Dislocation lines ⑦ and ⑧ are annihilated after reacting with each other, and satisfy the following equation:

$$\frac{1}{6}[2\bar{1}\bar{1}]+\frac{1}{6}[\bar{2}11]=0. \tag{13}$$

The dislocation line ⑨ is dissociated into dislocation lines ⑩ and ⑪, and obeys the following equation:

$$\frac{1}{2}[\bar{1}10]=\frac{1}{6}[\bar{1}2\bar{1}]+\frac{1}{6}[\bar{2}11]. \tag{14}$$

In addition to the interactions between the dislocations, the DLs are also twisted and distorted. As marked by the red dashed circle in Fig. 9, the DLs intertwine with each other to form two DLs.

Dislocation reactions occur repeatedly during solidification, which leads the dislocation lines to fluctuate as shown in Fig. 7. Dislocation reactions are dominated by Eqs. (3)–(6), at the cooling rate of 5×10^{11} K/s, so that $1/6\langle 112\rangle$ (Shockley) and $1/2\langle 110\rangle$ (perfect) dislocations are most abundant in the system. The dislocation reactions are relatively weak, which mainly change by climbing and distortion of their dislocation lines at the cooling rate of 1×10^{12} K/s.

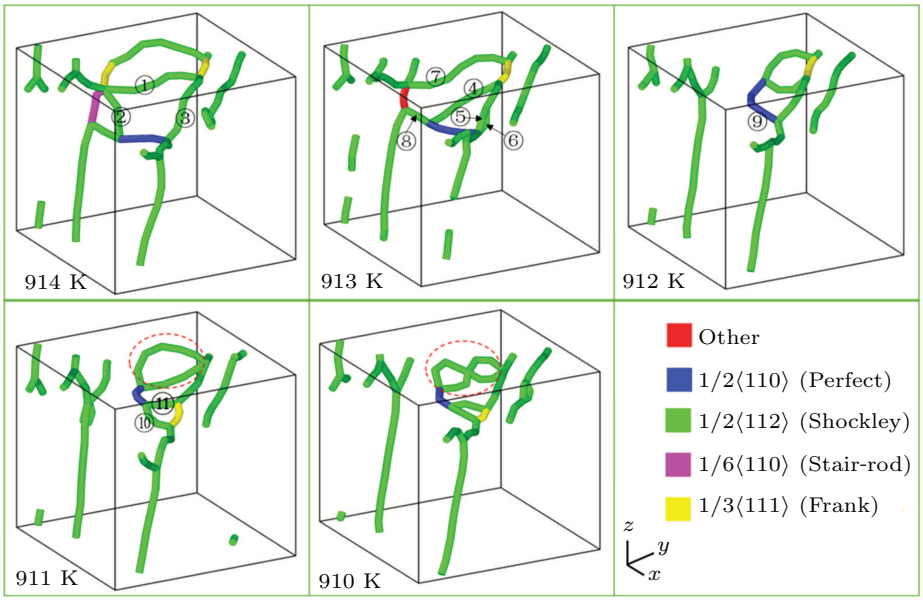


Fig. 9. Dislocation evolutions with temperature in a temperature range of 914 K–910 K at cooling rate 1×10^{12} K/s.

3.4.4. Dislocation-twin interactions

The stacking fault energy (SFE) of metal and alloy can control the deformation mechanism,[52] such as dislocation slip, deformation twinning, and phase transformation, while Ni–Co alloy has lower SFE,[53] and they are more prone to dislocation motion and phase transformation. Figures 10 and 11 show the formation of twins at the cooling rates of 5×10^{11} K/s and 1×10^{12} K/s, respectively.

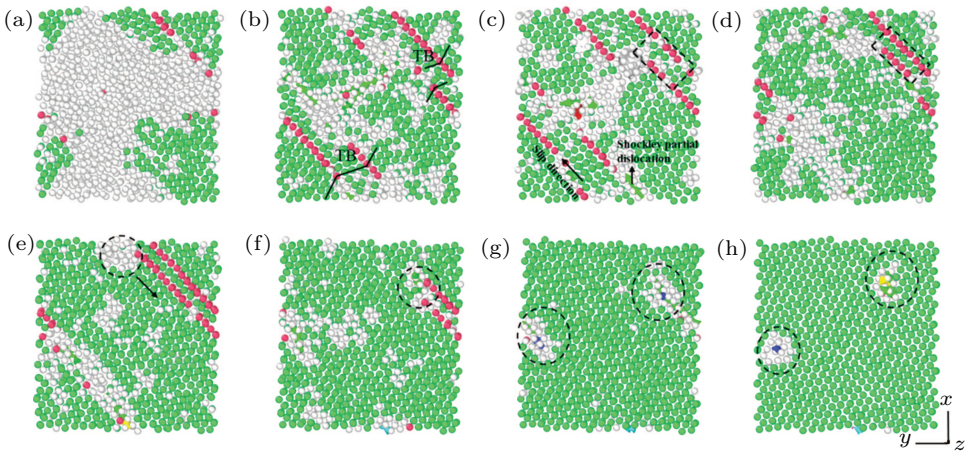


Fig. 10. Schematic diagrams of twin nucleation and detwinning slices at the cooling rate of 5×10^{11} K/s and temperatures: (a) 1420 K, (b) 1394 K, (c) 1367 K, (d) 1312 K, (e) 1296 K, (f) 1175 K, (g) 809 K, and (h) 300 K, with atomic colors representing FCC (green), HCP (red), and other (gray), with dislocation colors denoting $1/6\langle112\rangle$ (Shockley, green), $1/2\langle110\rangle$ (perfect, blue), $1/3\langle111\rangle$ (Frank, cyan), $1/3\langle001\rangle$ (Hirth, yellow), and other (red).

As shown in Figs. 10(a) and 10(b), for the cooling rate of 5×10^{11} K/s, substantial amorphous atoms gradually transform into FCC atoms during solidification, and meanwhile, many HCP TBs are formed. As shown in Figs. 10(c)–10(g), the $1/6\langle112\rangle$ (Shockley) partial dislocations generated in the front of TBs slip in the opposite direction of TBs growth, resulting in the shortening and eventual disappearance of TBs. As shown in the dashed box in Figs. 10(c) and 10(d), there is a reversible phase transition of HCP/FCC caused mainly by the slip of $1/6\langle112\rangle$ (Shockley). The partial dislocations affect the FCC/HCP phase boundary, causing the original HCP layer to transform into FCC and to convert the original FCC layer into HCP, which makes the thickness of TBs change from the original four atomic layers to three atomic layers. As shown in Figs. 10(e) and 10(f), partial dislocations continue to slip to make TBs shorter, and finally TBs disappear at $T = 809$ K, which is consistent with the experimental result observed by Li *et al.* by using EBSD and TEM.[54] The instability caused by thermal fluctuations at the solid-liquid interface leads the TBs to form, and the thinning and shortening of TBs is called detwinning.[55] As shown in the dashed circles in Figs. 10(g) and 10(h), after the disappearance of TBs, the region of the

other aggregation has higher energy and becomes a source of dislocations, which stimulates $1/2\langle 110\rangle$ (perfect) dislocations and fixed $1/3\langle 100\rangle$ (Hirth) dislocations. There are no TBs in the system eventually, and dislocations are concentrated in the high-energy amorphous regions.

At the early stage of crystallization at the cooling rate of 1×10^{12} K/s, massive amorphous structures gradually transform into FCC crystal atoms and a few HCP structure atoms form TBs as shown in Figs. 11(a)–11(c), TBs start to become longer and even penetrate the whole grain as the degree of crystallization deepens. The gray atoms in the front of TBs gradually transform into FCC, and that in the same layer with the TBs transforms into HCP, finally forming two perfect TBs at $T = 300$ K. These two TBs form the coherent twin boundary (CTB).[56] It is remarkable that the slip of the $1/6\langle 112\rangle$ (Shockley) partial dislocation at the TB terminal leads the FCC and HCP to stay in the same atomic layer, forming a "broken" TB, as illustrated by the dashed circles in Figs. 11(c) and 11(d). The dislocation exists at the FCC/HCP phase boundary due to the hindering effect of TB on the slip of the dislocation in Fig. 11(e), which is the main distribution pattern of dislocations at the cooling rate of 1×10^{12} K/s.

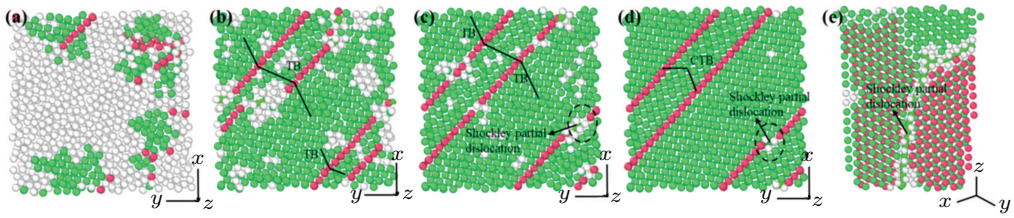


Fig. 11. Schematic diagrams of twin nucleations at cooling rate of 1×10^{12} K/s and temperatures: (a) 1260 K, (b) 1230 K, (c) 1140 K, (d) 300 K, and (e) dislocation distribution at the FCC/HCP phase boundary, with atomic colors representing FCC (green), HCP (red), and other (gray).

The abundant TBs in the alloy act as an effective barrier to the slip of dislocations, which improves their strength and electrical conductivity. When dislocations encounter TBs during slip, dislocations accumulate and rearrange. As a result, a large number of dislocations accumulate at TBs, which contributes to the pegging of dislocations. This microstructure evolution enhances the dislocation strengthening mechanism, which can greatly promote the hardness and strength of the alloy.[57]

4. Conlusions

Molecular dynamics simulations of $Ni_{47}Co_{53}$ alloy are performed by EAM potential function during rapid solidification, and the microstructure evolution mechanism and dislocation mechanism are investigated at five cooling rates of 1×10^{11} K/s, 5×10^{11} K/s, 1×10^{12} K/s, 5×10^{12} K/s, and 1×10^{13} K/s. The analysis focused on the dislocation evolutions and reactions at cooling rates of 5×10^{11} K/s and 1×10^{12} K/s, and some conclusions are drawn from this work as follows.

(i) FCC single crystals are formed at cooling rates of 1×10^{11} K/s and 5×10^{11} K/s, and polycrystalline with HCP TBs is formed at the cooling rate of 1×10^{12} K/s, and the crystalline and amorphous coexistance is realized at the cooling rate of 5×10^{12} K/s, and MGs are formed at the fastest cooling rate of 1×10^{13} K/s. The higher cooling rate exhibits lower crystallization temperature, as well as the smaller proportion of FCC, resulting in lower crystallinity.

(ii) The dislocations are relatively rare and formed only in the region with high energy at a cooling rate of 1×10^{11} K/s. The dislocations are scattered and the total dislocation length is also short at 5×10^{12} K/s. At 1×10^{13} K/s, the dislocation length is close to 0. The basically identical dislocation length is available for 5×10^{11} K/s and 1×10^{12} K/s, and the dislocations of the former are distributed in the region where the other atoms are aggregated, while those of the latter are distributed near the twin boundaries.

(iii) The $1/6\langle 112\rangle$ (Shockley) dominates at both cooling rates of 5×10^{11} K/s and 1×10^{12} K/s. The $1/2\langle 110\rangle$ (perfect) (about 40 Å) and $1/6\langle 110\rangle$ (stair-rod) (about 25 Å) are formed at 5×10^{11} K/s, and the dislocation fluctuations are more severe. Some other dislocations are formed at 1×10^{12} K/s, and the dislocation fluctuations are more stable. A multitude of dislocation reactions exist in both systems during rapid solidification, in which the interconversion between $1/6\langle 112\rangle$ (Shockley) and $1/2\langle 110\rangle$ (perfect) is dominant, and this reaction occurs repeatedly, while the reactions are more intense at 5×10^{11} K/s.

(iv) At 5×10^{11} K/s, the slip of partial dislocations leads to the disappearance of TBs, and stimulates the perfect and fixed dislocations, and there is no TBs in the system. The TBs are formed in the system at 1×10^{12} K/s, which creates FCC and HCP in the same atomic layer, and dislocations are formed at the junction. The interactions between dislocations and TBs affect the crystal structure. On the one hand, dislocations promote the formation and disappearance of TBs. On the other hand, TBs hinder the dislocations from moving.

Acknowledgements

Project supported by the National Natural Science Foundation of China (Grant Nos. 11964005, 11963003, and 62163006), the Fostering Project of Guizhou Univer-

sity, China (Grant Nos. [2020]33 and [2020]76), the Basic Research Program of Guizhou Province, China (Grant Nos. ZK[2022] 042 and ZK[2022] 143), and the Industry and Education Combination Innovation Platform of Intelligent Manufacturing and Graduate Joint Training Base at Guizhou University, China (Grant No. 2020-520000-83-01-324061).

References

[1] Correia A N and Machado S A S 2003 *J. Appl. Electrochem.* **33** 367
[2] Golodnitsky D, Rosenberg Y and Ulus A 2002 *Electrochimica Acta* **47** 2707
[3] Bai A and Hu C C 2002 *Electrochimica Acta* **47** 3447
[4] Burzyńska L and Rudnik E 2000 *Hydrometallurgy* **54** 133
[5] Thompson A W and Saxton H J 1973 *Metall. Trans.* **4** 1599
[6] Celebi O K, Mohammed A S K, Krogstad J A and Sehitoglu H 2022 *Int. J. Plast.* **148** 103141
[7] Koehler J 1941 *Phys. Rev.* **60** 397
[8] Schoeck G 1956 *Adv. Appl. Mech.* **4** 229
[9] Cottrell A H 1953 *Prog. Met. Phys.* **4** 205
[10] Lu L, Shen Y, Chen X, Qian L and Lu K 2004 *Science* **304** 422
[11] Laplanche G, Kostka A, Reinhart C, Hunfeld J, Eggeler G and George E P 2017 *Acta Mater.* **128** 292
[12] Miao J, Slone C E, Smith T M, Niu C, Bei H, Ghazisaeidi M, Pharr G M and Mills M J 2017 *Acta Mater.* **132** 35
[13] Zhang H, Wei B Q, Ou X Q, Ni S, Zhou K C and Song M 2022 *J. Phys. Chem. Solids* **169** 110835
[14] Mohammed A S K and Sehitoglu H 2020 *Acta Mater.* **183** 93
[15] Zhou N G, Wu X Y, Wei X Q, Zhou L, Wan Y P and Hu D L 2016 *J. Cryst. Growth* **443** 15
[16] Ryningen B, Stokkan G, Kivambe M, Ervik T and Lohne O 2011 *Acta Mater.* **59** 7703
[17] Xu J, Wang C B, Zhang W, Ren C L, Gong H F and Huai P 2016 *Chin. Phys. Lett.* **33** 026102
[18] Zhu C X and Yu T 2020 *Chin. Phys. B* **29** 096101
[19] Yu B Y, Liang Y C, Tian Z A, Liu R S, Gao T H, Xie Q and Mo Y 2020 *J. Cryst. Growth* **535** 125533
[20] Liang Y C, Xian G, Zhou L L, Tian Z A, Chen Q, Mo Y F, Liu R S, Gao T H, Xie Q and He M 2022 *J. Alloys Compd.* **891** 161953
[21] Zhang D E, Zhou L L, Liang Y C, Tian Z A, Liu R S, Gao T H, Xie Q and Chen Q 2020 *CrystEngComm* **22** 7888
[22] Ma R B, Zhou L L, Liang Y C, Chen Q, Tian Z A, Liu R S, Mo Y F, Gao T H and Xie Q 2021 *Curr. Appl. Phys.* **29** 18
[23] Plimpton S 1995 *J. Comput. Phys.* **117** 1
[24] Pun G P, Yamakov V and Mishin Y 2015 *Model. Simul. Mater. Sci. Eng.* **23** 065006
[25] Mihalkovič M and Widom M 2007 *Phys. Rev. B* **75** 014207
[26] Mishin Y 2004 *Acta Mater.* **52** 1451
[27] Pun G P and Mishin Y 2012 *Phys. Rev. B* **86** 134116
[28] Zhao S, Zhang Y and Weber W J 2018 *Scr. Mater.* **145** 71
[29] Zhang Y, Jin K, Xue H, Lu C, Olsen R J, Beland L K, Ullah M W, Zhao S, Bei H and Aidhy D S 2016 *J. Mater. Res.* **31** 2363
[30] Shaipov R K, Kerimov E Y and Slyusarenko E M 2017 *J. Alloys Compd.* **701** 262
[31] William G and Hoover 1985 *Phys. Rev. A* **31** 1695
[32] Nosé S 1984 *J. Chem. Phys.* **81** 511
[33] Parrinello M and Rahman A 1981 *J. Appl. Phys.* **52** 7182
[34] Stukowski A 2009 *Model. Simul. Mater. Sci. Eng.* **18** 015012
[35] Stukowski A 2012 *Model. Simul. Mater. Sci. Eng.* **20** 045021
[36] Stukowski A and Albe K 2010 *Model. Simul. Mater. Sci. Eng.* **18** 085001
[37] Dunitz J D 1991 *Pure Appl. Chem.* **63** 177
[38] Fukasawa T and Sato T 2011 *Phys. Chem. Chem. Phys.* **13** 3187
[39] Liang K, Dong F, Wu G and Liu S 2021 *Mater. Sci. Semicond. Process.* **121** 105340
[40] Liu C S, Xia J, Zhu Z G and Sun D Y 2001 *J. Chem. Phys.* **114** 8
[41] Schroers J and Paton N 2006 *Adv. Mater. Process.* **164** 61
[42] Penn R L and Banfield J F 1998 *Science* **281** 969
[43] Kalikmanov V I 2013 *Nucleation theory* (Dordrecht: pringer) pp. 17–41
[44] Zanotto E D and James P F 1985 *J. Non-Cryst. Solids* **74** 373
[45] Gleiter H 1991 *Advanced Structural and Functional Materials*, ed. Bunk W G J (Berlin, Heidelberg: Springer) pp. 1–37
[46] Inoue T, Watanabé J and Yamamoto M 1974 *J. Cryst. Growth* **24** 418
[47] Kroupa F 1960 *Cechoslov- Fiz. Zurnal B* **10** 284
[48] Zhang Y Q, Jiang S Y, Zhu X M and Zhao Y N 2017 *Phys. E Low-Dimens. Syst. Nanostructures* **90** 90
[49] Hirth J P 1994 *J. Phys. Chem. Solids* **55** 985
[50] Bulatov V V, Hsiung L L, Tang M, Arsenlis A, Bartelt M C, Cai W, Florando J N, Hiratani M, Rhee M and Hommes G 2006 *Nature* **440** 1174
[51] Kusov A A and Vladimirov V I 1986 *Phys. Status Solidi B* **138** 135
[52] Christian J W and Mahajan S 1995 *Prog. Mater. Sci.* **39** 1
[53] Tian C, Xu L, Cui C and Sun X 2015 *Metall. Mater. Trans. A* **46** 4601
[54] Li B Q, Sui M L, Li B, Ma E and Mao S X 2009 *Phys. Rev. Lett.* **102** 205504
[55] Zhao F, Wang L, Fan D, Bie B X, Zhou X M, Suo T, Li Y L, Chen M W, Liu C L and Qi M L 2016 *Phys. Rev. Lett.* **116** 075501
[56] Jin Z H, Gumbsch P, Ma E, Albe K, Lu K, Hahn H and Gleiter H 2006 *Scr. Mater.* **54** 1163
[57] Wei H, Chen Y, Li Z, Shan Q, Yu W and Tang D 2021 *Mater. Sci. Eng. A* **826** 142023